UDC 624.04
DOI: 10.15587/2706-5448.2023.274348

Sabah Moussaoui, Chabane Rebadj, Mourad Belgasmia, Kong Fah Tee

A STUDY OF MESH INFLUENCE ON EXTENDED FINITE ELEMENT CRACKED PLATE AND FINITE ELEMENT PLATE BENDING

The object of this study is a refining mesh effect on discontinuous structures response.

This paper presents a study of mesh influence between cracked and non-cracked plates using extended finite element and standard finite element method, respectively. For the first case, the plate is stressed on one side, in which cracked zone displacements are given for different mesh refinements. The second case study is bending orthotropic and isotropic plates under uniform rectangular impulsive load, in which mesh influence on the structural response is presented. The numerical modelization is done using an isoperimetric quadrilateral element. On one hand, the stiffness linear matrix of a cracked plate is evaluated numerically by adding an enriched shape function to the standard shape function to be able to model discontinuity numerically. On the other hand, for the case of the non-cracked plate, the use of the finite element method with standard shape function is well suited to the numerical design of stiffness and mass matrix.

The essence of this study is to show the mesh effect on cracked and non-craked plate response, which is a first step that allows to go even further on monoitoring of our crack evolution.

It is a very useful field as any structure in our daily life is subject to a discontinuity (crack) which we must be able to control in order to evoid a future structure collapse.

Keywords: *extended finite element method (XFEM), finite element method (FEM), crack, transient analysis, plate.*

Received date: 13.01.2023
Accepted date: 19.02.2023
Published date: 24.02.2023

How to cite
Moussaoui, S., Rebadj, C., Belgasmia, M., Tee, K. F. (2023). A study of mesh influence on extended finite element cracked plate and finite element plate bending. Technology Audit and Production Reserves, 1 (1 (69)), 6–12. doi: https://doi.org/10.15587/2706-5448.2023.274348

1. Introduction

Researchers are led to use numerical methods and modelization for the increasing complexity of structural mechanics problems. Knowing that finite element method is without a doubt the most powerful method for structural analysis, and the most common numerical tool, which allows the approximate solutions of partial differential equations. This later has been applied successfully in many complex structures, which are not easily calculated by the usual procedures of resistance of structures, such as plates and shells. This does not mean that it has not shown its limits in certain fields.

Finite Element Methods approximations are piecewise differentiable polynomial approximations, which are illusuited to represent problems with discontinuities (either in the Unknown field or its gradient), singularities and boundary layers. To accurately model discontinuities with finite element methods, it is necessary to conform the discretization (mesh) to the line or surface of discontinuity. This becomes a major difficulty when treating problems with evolving discontinuities where the mesh must be regenerated at each step. In standard finite element methods, singularities or boundary layers are resolved by requiring significant mesh refinement in the regions where the gradients of the fields are large.

It is possible to say that the finite element method relies on polynomials approximation properties, so they often require smooth solutions to achieve optimal accuracy. However, if the solution contains strong discontinuities in the displacement field as in the case of cracked bodies, then the finite element method becomes computationally expensive. Hence the emergence of the extended finite element method (XFEM), which is a numerical technique that enables the incorporation of local enrichment approximation to overcome the limits facing the finite element method, by enriching the standard shape functions using Heaviside and Branch functions allowing a numerical modelization of discontinuities [1–6]. Recently a lot of work in this field has been done by [7, 8].

One of the most awkward problems encountered in the analyses of crack growth is that remeshing is required near the crack tip as the crack grows. Such remeshing is not only burdensome.

The aim of this research is to know if there is a refining mesh effect on discontinuous structures response as is the case for continuous one, by the use of the extended finite element method to apprehend the problem that the finite element method cannot solve, namely, a cracked plate stressed on one side and embedded on another side, with a central crack. In addition, the use of the finite element

method for dynamic analysis of orthotropic and isotropic plates under uniform rectangular impulsive load is studied using temporal step-by-step integration.

2. Materials and Methods

The object of this research is a refining mesh effect on discontinuous structures response.

2.1. Extended finite element formulation. Knowing that discontinuity surfaces may cut the finite elements, in this case it is necessary to enrich the elements cut by a discontinuity with new functions at different crack zone. Crack modelling using Extended Finite Element Method includes two types of enrichment: an enrichment for the front of the crack using branch functions characterizing the asymptotic behaviour displacement field near the crack front [1] and an enrichment for the interior of the crack using a step function with value 1.0 above the crack and –1.0 below [9]. The fact that a node is enriched or not and the type of enrichment depends on the relative position of its support relative to the crack [10–14] as shown in Fig. 1.

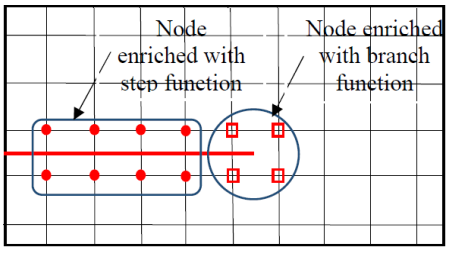

Fig. 1. Step and branch function enriched node

The 2D modelling of the displacement field can be written as follows:

$$u^h(x)=\sum_{I\in N}N_I(x)u_I+\sum_{J\in N_{er}}\tilde{N}_J(x)\big(H(x)-H(x_J)\big)a_J+$$

$$+\sum_{J\in N_{tip}}\tilde{N}_K(x)\sum_{\alpha=1}^{4}\big(B_\alpha(x)-B_\alpha(x_K)\big)b_{\alpha K}, \quad (1)$$

where $N_I(x)$, $\tilde{N}_J(x)$, $\tilde{N}_K(x)$ – standard finite element shape function; $B_\alpha(x)$ – branch function; $H(x)$ – Heaviside step function:

$$H(x)=\begin{cases}+1, & \text{above the crack,}\\ -1, & \text{bellow the crack.}\end{cases}$$

The standard part of the approximation is:

$$u_i(x)=\sum_{I\in N}N_I(x)U_{Ii}, \quad (2)$$

where N – set of nodes constituting the mesh; $N_I(x)$ – shape function associated with node I, note that $N_I(x_I)=\delta_{IJ}$; x_I – node I coordinates; U_{Ii} – nodal unknown of node I for the i^{th} component. The enriched approximation field is:

$$u_i(x)=\sum_{I\in N}N_I(x)U_{Ii}+$$

$$+\sum_{J\in P.U.}f_J(x)\psi(x)A_{Ji}, \quad (3)$$

where $P.U.$ – set of functions building the partition of unity; $f_J(x)$ – function of the partition of unity; $\psi(x)$ – enriched or additional function; A_{Ji} – additional unknowns associated with the function $f_J(x)$.

If to take all the additional unknowns A_{Ji} equal to 1 and all the standard nodal unknowns U_{Ii} equal to zero, the approximation can recover the additional function $\psi(x)$. The support of the partition of unity is called Ω^{PU}. This support is usually located around the discontinuity but it can be extended if one needs to model a high gradient; as in the case of a crack tip.

This last expression is not the standard expected relation where the nodal is the real unknown U_{Ki}; displacement on the node. To satisfy this relation, the following approximation is often used:

$$u_i(x)=\sum_{I\in N}N_I(x)U_{Ii}+\sum_{J\in N^{enr}.}N_J(x)\big(\psi(x)-\psi(x_J)\big)A_{Ji}. \quad (4)$$

2.2. Extended finite element plate formulation. The strain tensor components, written as a vector is:

$$\{\varepsilon\}=\begin{bmatrix}\varepsilon_{xx}\\ \varepsilon_{yy}\\ 2\varepsilon_{xy}\end{bmatrix}=[D]\{U^e(M)\} \text{ with } [D]=\begin{bmatrix}\frac{\partial}{\partial x} & 0\\ 0 & \frac{\partial}{\partial y}\\ \frac{\partial}{\partial y} & \frac{\partial}{\partial x}\end{bmatrix}. \quad (5)$$

Numerical implementation by replacing $\{U^e(M)\}$ using its approximated form leads to:

$$\{\varepsilon\}=[D][N^e(M)]\{q^e\}=[B^e(M)]\{q^e\}, \quad (6)$$

where $[B^e(M)]$ is the discretized gradient operator, it contains both standard part and enriched part as written:

$$[B^e(M)]=[B^e_{std}(M)\ B^{enr}_{std}(M)]. \quad (7)$$

The shape function N_I (I from 1 to 4) are bi-linear in ξ and η (coordinates in the parent element) [15]:

$$N_1(\xi,\eta)=\frac{1}{4}(1-\xi)(1-\eta),\ N_2(\xi,\eta)=\frac{1}{4}(1+\xi)(1-\eta), \quad (8)$$

$$N_3(\xi,\eta)=\frac{1}{4}(1+\xi)(1+\eta),\ N_4(\xi,\eta)=\frac{1}{4}(1-\xi)(1+\eta). \quad (9)$$

In Equation (7), the discretized gradient operator $[B^e_{std}(M)]$ is equal to:

$$[B^e_{std}(M)]=\begin{bmatrix}N_{1,x} & N_{2,x} & N_{3,x} & N_{4,x} & 0 & 0 & 0 & 0\\ 0 & 0 & 0 & 0 & N_{1,y} & N_{2,y} & N_{3,y} & N_{4,x}\\ N_{1,y} & N_{2,y} & N_{3,y} & N_{4,y} & N_{1,x} & N_{2,x} & N_{3,x} & N_{4,x}\end{bmatrix}. \quad (10)$$

The enriched discretized gradient operator $[B^e_{enr}(M)]$ is equal to:

$$[B^e_{std}(M)]=$$

$$=\begin{bmatrix}(N_1\psi_1)_{,x} & (N_2\psi_2)_{,x} & (N_3\psi_3)_{,x} & (N_4\psi_4)_{,x} & 0 & 0 & 0 & 0\\ 0 & 0 & 0 & 0 & (N_1\psi_1)_{,y} & (N_2\psi_2)_{,y} & (N_3\psi_3)_{,y} & (N_4\psi_4)_{,y}\\ (N_1\psi_1)_{,y} & (N_2\psi_2)_{,y} & (N_3\psi_3)_{,y} & (N_4\psi_4)_{,y} & (N_1\psi_1)_{,x} & (N_2\psi_2)_{,x} & (N_3\psi_3)_{,x} & (N_4\psi_4)_{,x}\end{bmatrix}. \quad (11)$$

 ISSN 2664-9969

In the case of a Heaviside enrichment, the derivative of $\psi(x)$ is zero, so the enriched gradient operator is:

$$\left[B^e_{std}(M)\right]= =\begin{bmatrix} N_{1,x}\psi_1 & N_{2,x}\psi_2 & N_{3,x}\psi_3 & N_{4,x}\psi_4 & 0 & 0 & 0 & 0 \\ 0 & 0 & 0 & 0 & N_{1,y}\psi_1 & N_{2,y}\psi_2 & N_{3,y}\psi_3 & N_{4,y}\psi_4 \\ N_{1,x}\psi_1 & N_{2,x}\psi_2 & N_{3,x}\psi_3 & N_{4,x}\psi_4 & N_{1,y}\psi_1 & N_{2,y}\psi_2 & N_{3,y}\psi_3 & N_{4,y}\psi_4 \end{bmatrix}. \quad (12)$$

Computation of $\partial y/\partial\xi$ and $\partial y/\partial\eta$ needs Jacobian:

$$J=\begin{bmatrix} \frac{\partial\xi}{\partial x} & \frac{\partial\xi}{\partial y} \\ \frac{\partial\eta}{\partial x} & \frac{\partial\eta}{\partial y} \end{bmatrix}.$$

$$x=\sum_{I=1}^{4} N_I x_I,\ \frac{\partial x}{\partial\xi}=\sum_{I=1}^{4}\frac{\partial N_I}{\partial\xi}x_I,\ \frac{\partial x}{\partial\eta}=\sum_{I=1}^{4}\frac{\partial N_I}{\partial\eta}x_I, \quad (13)$$

$$y=\sum_{I=1}^{4} N_I y_I,\ \frac{\partial y}{\partial\xi}=\sum_{I=1}^{4}\frac{\partial N_I}{\partial\xi}y_I,\ \frac{\partial y}{\partial\eta}=\sum_{I=1}^{4}\frac{\partial N_I}{\partial\eta}y_I. \quad (14)$$

The expression of stiffness matrix for an enriched element is:

$$\left[K\right]^e=\int_{\Omega^e}\left[B^e\right]^T\left[D^e\right]\left[B^e\right]\mathrm{d}\Omega= =\int_{-1}^{1}\int_{-1}^{1}\int_{\Omega^e}\left[B^e(\xi,\eta)\right]^T\left[D^e\right]\left[B^e(\xi,\eta)\right]\det[J]\,\mathrm{d}\xi\mathrm{d}\eta, \quad (15)$$

where $\left[D^e\right]$ is the material law. The stiffness matrix can be decomposed into blocs as presented below:

$$\left[K\right]^e_l=\begin{bmatrix} \int_{\Omega^e}\left[B^e_{std}\right]^T\left[D^e\right]\left[B^e_{std}\right]\mathrm{d}\Omega & \int_{\Omega^e}\left[B^e_{std}\right]^T\left[D^e\right]\left[B^e_{enr}\right]\mathrm{d}\Omega \\ \int_{\Omega^e}\left[B^e_{enr}\right]^T\left[D^e\right]\left[B^e_{std}\right]\mathrm{d}\Omega & \int_{\Omega^e}\left[B^e_{enr}\right]^T\left[D^e\right]\left[B^e_{enr}\right]\mathrm{d}\Omega \end{bmatrix}. \quad (16)$$

2.3. Plate displacement and deformation field description. Plate displacement is based on three independent variables: transverse displacement and two rotations written as follows:

$$u=z\beta_x(x,y),\ v=z\beta_y(x,y),\ w=w(x,y). \quad (17)$$

The deformation field with bending and shear effects can be presented below:

– contribution of bending effect:

$$\left\{\varepsilon_f\right\}=\begin{Bmatrix}\varepsilon_{xx}\\ \varepsilon_{yy}\\ \gamma_{xy}\end{Bmatrix}=z\left\{\chi\right\}=z\begin{Bmatrix} \frac{\partial\beta_x}{\partial x} \\ \frac{\partial\beta_y}{\partial y} \\ \frac{\partial\beta_x}{\partial y}+\frac{\partial\beta_y}{\partial x}\end{Bmatrix}; \quad (18)$$

– contribution of shear effect:

$$\left\{\varepsilon_c\right\}=\left\{\gamma\right\}=\begin{Bmatrix}\gamma_{xz}\\ \gamma_{yz}\end{Bmatrix}=\begin{Bmatrix}\beta_x+\frac{\partial w}{\partial x}\\ \beta_y+\frac{\partial w}{\partial y}\end{Bmatrix}. \quad (19)$$

Motion equations formulation can be given by Lagrange's equations using kinetic, potential energy [16–18] expressed as follows:

$$T=\frac{1}{2}\sum_{i=1}^{n}\sum_{j=1}^{n}\dot{q}_i\,M_{ij}\,\dot{q}_j=\frac{1}{2}\,\dot{q}^T M\,\dot{q},$$

$$U=\frac{1}{2}\sum_{i=1}^{n}\sum_{j=1}^{n}q_i\,K_{ij}q_j=\frac{1}{2}q^T K\,q. \quad (20)$$

Using Lagrange's equations, which is:

$$\frac{\partial}{\partial t}\left(\frac{\partial T}{\partial\dot{q}_i}\right)-\frac{\partial T}{\partial q_i}+\frac{\partial U}{\partial q_i}=F_i(t). \quad (21)$$

Thus equation motion can be written as below:

$$\left[M\right]\{\ddot{q}\}+\left[K\right]\{q\}=\{F(t)\}, \quad (22)$$

where $\left[M\right]$ – global mass matrix; $\left[K\right]$ – global stiffness matrix; $\{F(t)\}$ – global external load vector.

2.4. Finite Element Plate Formulation. Bending interpolation and shear deformations matrix can be written as follow:

$$\{\chi\}=\left\{\bar{\varepsilon}_f\right\}=\begin{bmatrix} 0 & \frac{\partial N^T}{\partial x} & 0 \\ 0 & 0 & \frac{\partial N^T}{\partial y} \\ 0 & \frac{\partial N^T}{\partial y} & \frac{\partial N^T}{\partial x}\end{bmatrix}\begin{Bmatrix}W\\ \hat{\beta}_x\\ \hat{\beta}_y\end{Bmatrix},$$

$$\{\varepsilon_c\}=\{\gamma\}=\begin{bmatrix} \frac{\partial N^T}{\partial x} & N^T & 0 \\ \frac{\partial N^T}{\partial y} & 0 & N^T\end{bmatrix}\begin{Bmatrix}W\\ \hat{\beta}_x\\ \hat{\beta}_y\end{Bmatrix}. \quad (23)$$

The constitutive matrix of the orthotropic plate takes the form:

$$\left[D_f\right]=\frac{h^3}{12}\begin{bmatrix} \frac{E_1}{1-\nu_{21}\nu_{12}} & \frac{E_2\nu_{12}}{1-\nu_{21}\nu_{12}} & 0 \\ \frac{E_2\nu_{12}}{1-\nu_{21}\nu_{12}} & \frac{E_2}{1-\nu_{21}\nu_{12}} & 0 \\ 0 & 0 & G_{12}\end{bmatrix},$$

$$\left[D_c\right]=hk\begin{bmatrix} G_{13} & 0 \\ 0 & G_{23}\end{bmatrix}, \quad (24)$$

where $\left[D_f\right]$ – bending constitutive matrix; $\left[D_c\right]$ – shear constitutive matrix; E_1, E_2 – Young moduli (x) and (y) directions respectively; ν_{12}, ν_{21} – Poisson's ratios; G_{12}, G_{13}, G_{23} – shear moduli; k – cross-shear correction coefficient.

Stiffness and mass matrix expression using deformation energy and Kinetic energy, respectively [16–19]:

$$\left[K\right]=\left[K_f\right]+\left[K_c\right]=\int_S\left[\bar{\beta}_f\right]^T\left[D_f\right]\left[\bar{\beta}_f\right]\mathrm{d}x\,\mathrm{d}y+ +\int_S\left[\beta_\gamma\right]^T\left[D_c\right]\left[\beta_\gamma\right]\mathrm{d}x\,\mathrm{d}y, \quad (25)$$

$$\left[K\right]=\int_{-1}^{+1}\int_{-1}^{+1}\left[\bar{\beta}_f\right]^T\left[D_f\right]\left[\bar{\beta}_f\right]\det[J]\,\mathrm{d}\xi\mathrm{d}\eta+ +\int_{-1}^{+1}\int_{-1}^{+1}\left[\beta_\gamma\right]^T\left[D_c\right]\left[\beta_\gamma\right]\det[J]\,\mathrm{d}\xi\mathrm{d}\eta, \quad (26)$$

$$[M_w]^e = \int_{S^e} \rho h [N]^{eT} [N]^e dS,$$

$$[M_\beta]^e = \int_{S^e} \rho \frac{h^3}{12} [N]^{eT} [N]^e dS,$$

$$[M]^e = \begin{bmatrix} [M_w]^e & [0] & [0] \\ [0] & [M_\beta]^e & [0] \\ [0] & [0] & [M_\beta]^e \end{bmatrix}, \quad (27)$$

where $[J]$ – Jacobian matrix; $[K_f]$ – bending stiffness matrix; $[K_c]$ – shear stiffness matrix; $[M]$ – mass matrix.

The load vector is expressed as follows:

$$\{F\}^e = \int_{V^e} [N]^T \{f_V\} dV + \int_{S^e} [N]^T \{f_S\} dS. \quad (28)$$

2.5. Resolution method. The approach under consideration, for second-order differential equations system resolution, is a direct resolution method [16–20].

The direct analysis of a structure in transitory mode implies step-by-step integration motion:

$$[M]\{\ddot{q}\} + [K]\{q\} = \{F(t)\}.$$

In this method; displacements, velocity and accelerations vector at time $T=0$ are known. The period T, over which the response is required, is subdivided in N intervals time and equalizes Δt. The use of this integration scheme establishes a solution approximation at times: Δt, $2\Delta t$,..., t, $t+\Delta t$,..., T. The resolution algorithm (Newmark's method) is represented in Table 1 which is divided into two parts.

Table 1

Step-by-step resolution algorithm

Step	Designation
A. Initial calculation	
1. Form stiffness and mass matrix	[K], [M]
2. Initialize	$\{q_0\}$, $\{\dot{q}_0\}$ and $\{\ddot{q}_0\}$
3. Select time step Δt, parameters α, β, and calculate integrations constants	$\alpha \geq 0.5$, $\beta \geq 0.25(0.5+\alpha)^2$, $a_0 = \frac{1}{\beta \Delta t^2}$, $a_1 = \frac{\alpha}{\beta \Delta t}$, $a_2 = \frac{1}{\beta \Delta t}$, $a_3 = \frac{1}{2\beta} - 1$
4. Form an effective stiffness matrix	$[\bar{K}] = [K] + a_0[M]$
5. Matrix triangularization	$[\bar{K}]: [\bar{K}] = LDL^T$
B. For each time step	
1. Calculate the effective load at time $t+\Delta t$	$\{\bar{F}_{t+\Delta t}\} = \{F_{t+\Delta t}\} + [M]\left[a_0\{q_t\} + a_2\{\dot{q}_t\} + a_3\{\ddot{q}_t\}\right]$
2. Solve in terms of displacement at time $t+\Delta t$	$LDL^T q_{t+\Delta t} = \bar{F}_{t+\Delta t}$
3. Calculate accelerations and velocity at the time $t+\Delta t$	$\{\ddot{q}_{t+\Delta t}\} = a_0\left(\{q_{t+\Delta t}\} - \{q_t\}\right) - a_2\{\dot{q}_t\} - a_3\{\ddot{q}_t\}$; $\{\dot{q}_{t+\Delta t}\} = \{\dot{q}_t\} + \Delta t\,(1-\alpha)\{\ddot{q}_t\} + \alpha\Delta t\{\ddot{q}_{t+\Delta t}\}$

3. Results and Discussion

3.1. Central crack of square plate. Consider a homogeneous isotropic square plate, with a width and height equal to 1 m, stressed by a distributed load: $\sigma=100$ KN/m^2 (Fig. 2), with a central crack length equal to 20 cm whose elastic properties are as follows: modulus of elasticity: $E=7\cdot10^6$ MPA, Poisson's ratio: $\upsilon=0.3$.

The 2D model of the cracked square plate is represented in Fig. 3.

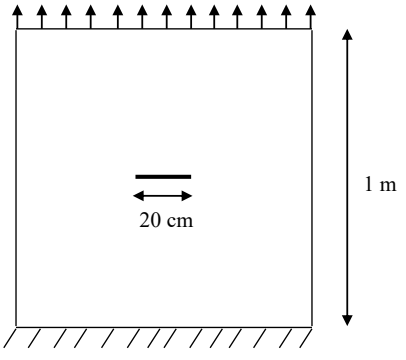

Fig. 2. Geometry of a homogeneous isotropic cracked square plate

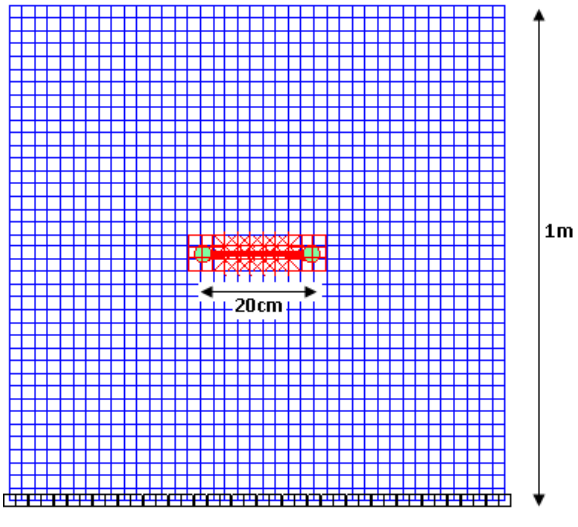

Fig. 3. 2D model of cracked square plate

The aim is to study a mesh refinement influence of cracked square plate under tension, on the top side and embedded on the bottom side. Results are represented in Fig. 4, which gives information about the numerical model with different meshes as well as stress and numerical deformed configuration corresponding to each mesh refinement. It is possible to notice in Fig. 4 that mesh refinement has a big influence on the cracked zone itself as well as the zone surrounding the crack.

3.2. Finite element example

3.2.1. Simply supported isotropic square plate. Let's consider an isotropic square plate, subjected to a uniform rectangular impulsive load, structure geometry and material properties are represented in Fig. 5.

Data:

– Initial condition: $a=2.438$ m; $P_0(x,y,t)=47.9$ N/m^2;

– $w=\dot{w}=0$: $E=6.897\cdot10^{10}$ N/m^2; $P_0(x,y,t)=48.82$ N/m^2;

– Newmark parameters: $\rho=254$ kg/m^3; $\nu=0.25$; $\alpha=1/2$, $\beta=1/4$ (Newmark). $\rho=254.7$ kg/m^3; $h=6.35\cdot10^{-3}$ m.

ISSN 2664-9969

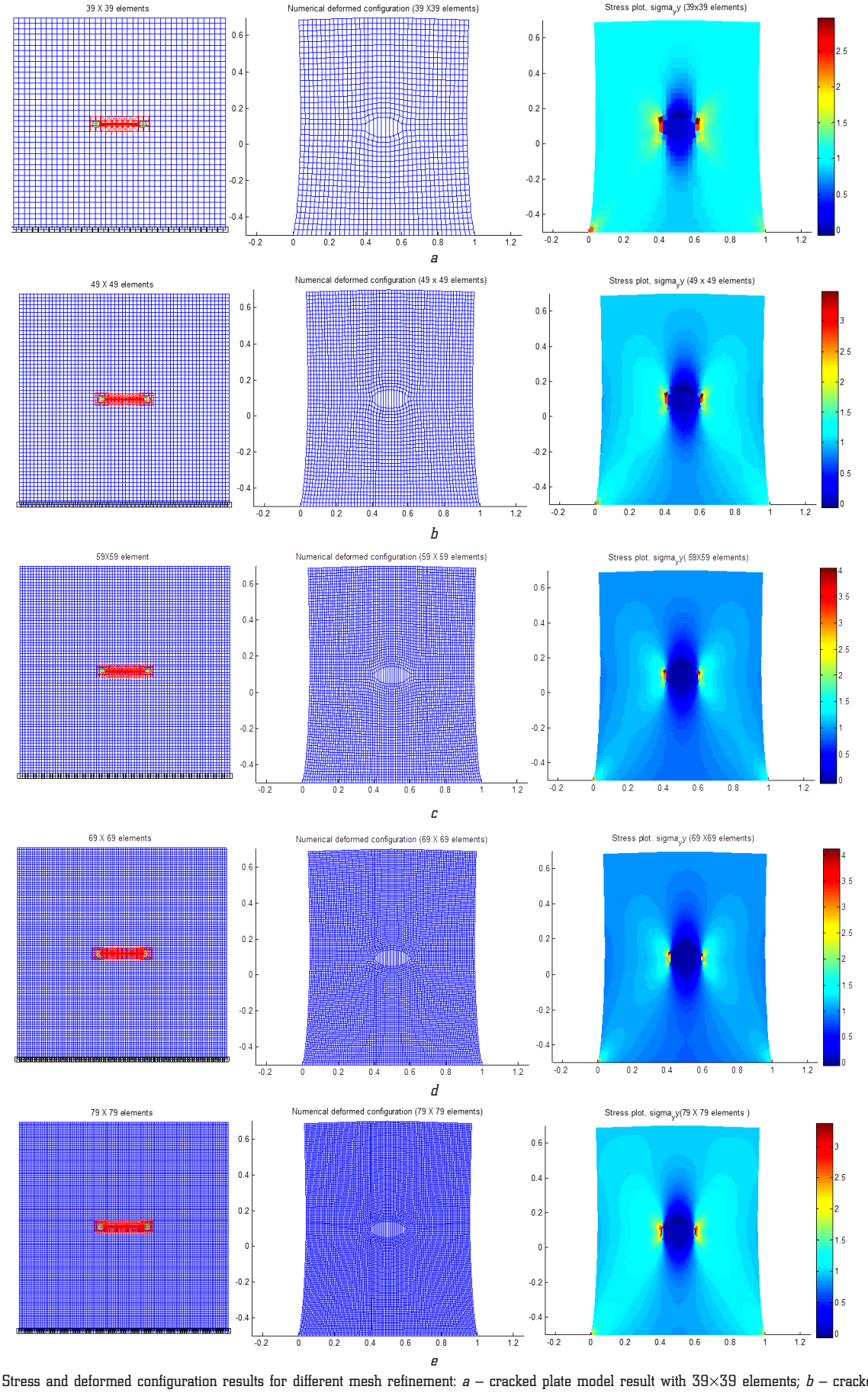

Fig. 4. Stress and deformed configuration results for different mesh refinement: *a* – cracked plate model result with 39×39 elements; *b* – cracked plate model result with 49×49 elements; *c* – cracked plate model result with 59×59 elements; *d* – cracked plate model result with 69×69 elements; *e* – cracked plate model result with 79×79 elements

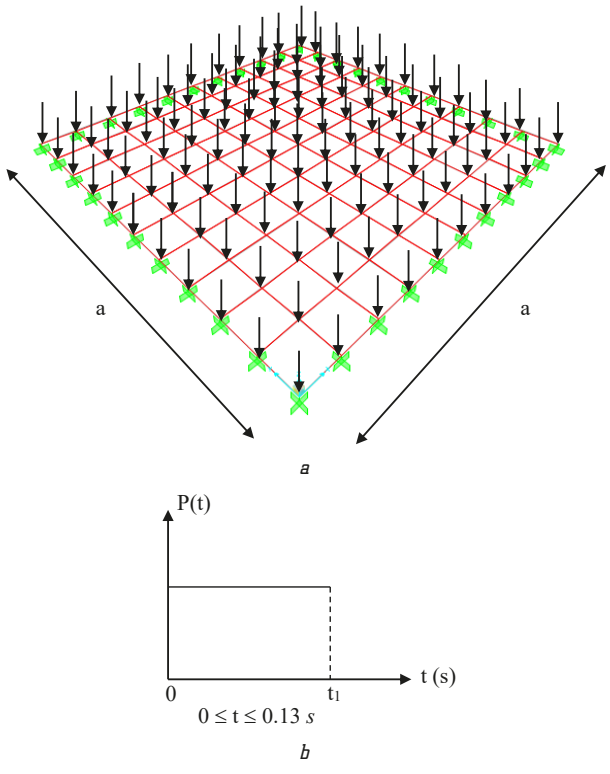

Fig. 5. Isotropic plate under uniform rectangular impulsive load: *a* – structure geometry; *b* – uniform rectangular impulsive load

3.2.2. Orthotropic square plate. For the second example, let's consider a thin orthotropic plate (corrugated aluminium plate), subjected to a rectangular impulsive load with intensity P, data plate information is presented below:

$a=1.5$ m; $E_1=30\cdot10^{10}$ N/m^2;

$\rho=2710$ kg/m^3; $E_2=0.8\cdot10^{10}$ N/m^2;

$h=7\cdot10^{-3}$ m; $G_{12}=G_{13}=G_{23}=0.375\cdot10^{10}$ N/m^2;

$P_0(x,y,t)=950$ N/m^2; $\nu_{12}=0.33$.

For a time step equal to 0.0025 s, and for the case of simple support, mesh influence is shown in Fig. 6.

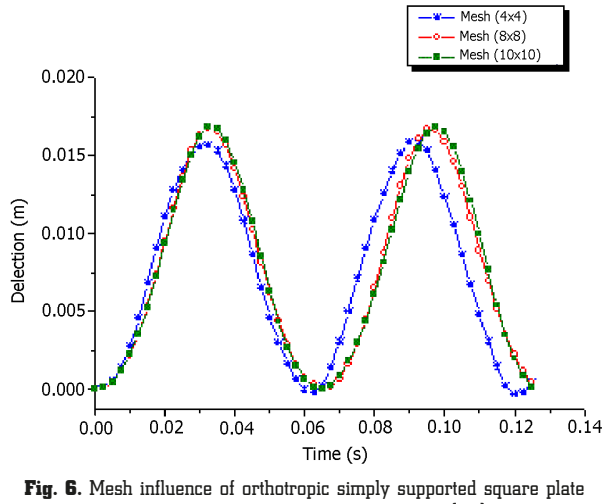

Fig. 6. Mesh influence of orthotropic simply supported square plate on the transient response displacement [20]

The first case is a square central cracked plate stressed on the top side and embedded on the bottom side, in which Fig. 4 shows a direct influence of mesh on stress results in both cracked zone and zone surrounding the crack using 39, 49, 59, 69 and 79 elements per side. It is possible to notice that more the mesh is refined, more lightened are the stress; on different level namely, cracked zone, non-cracked zone and crack tip.

The second case is the study of mesh influence for the isotropic and orthotropic non-cracked plates under uniform rectangular impulsive load. Table 2 and Fig. 6 indicate the maximum normal displacement amplitude and transient response displacement values in the plate centre according to mesh using 4, 6, 8 and 10 elements per side, respectively.

Table 2

Maximum deflection amplitude of simply supported isotropic plate according to mesh with the time step $\Delta t=0.005$ s

Mesh	(4×4)	(6×6)	(8×8)	(16×16)
Newmark (Q4) displacement (cm)	0.85858	0.86662	0.88252	0.88801
Newmark (DKT) displacement (cm) [19]	0.80853	0.85401	0.86588	0.88258
HHT displacement (cm) [19]	0.82756	0.86261	0.88344	0.89498

Knowing that Finite Element Methods approximations are piecewise differentiable polynomial approximations, which are ill-suited to represent problems with discontinuities (either in the Unknown field or its gradient), singularities and boundary layers, extended finite element method is well suited for disocntinuities modeling.

4. Conclusions

This work sheds light on the mesh effect on structures whether cracked or not, starting by using an elegant method that allows numerical modelization of cracks. Finite element methods approximations are piecewise differentiable polynomial approximations, which are ill-suited to represent problems with discontinuities. Hence the emergence of the extended finite element method to overcome the limits presented by the finite element method.

Using the two methods (extended finite element and finite element) for cracked and non-cracked plates, respectively, it is possible to conclude that there is a direct mesh influence on stress results whether in the cracked zone and around, using 39, 49, 59, 69 and 79 elements per side, as well as a big mesh influence for non-crack isotropic and orthotropic plate in dynamic transient response.

Conflict of interest

The authors declare that they have no conflict of interest in relation to this research, whether financial, personal, authorship or otherwise, that could affect the research and its results presented in this paper.

Financing

The study was performed without financial support.

Presentation of research in the form of publication through financial support in the form of a grant from SUES (Support to Ukrainian Editorial Staff).

ISSN 2664-9969

Data availability

The manuscript has no associated data.

References

1. Belytschko, T., Black, T. (1999). Elastic crack growth in finite elements with minimal remeshing. *International Journal for Numerical Methods in Engineering, 45 (5),* 601–620. doi: https://doi.org/10.1002/(sici)1097-0207(19990620)45:5<601::aid-nme598>3.0.co;2-s
2. Zi, G., Belytschko, T. (2003). New crack-tip elements for XFEM and applications to cohesive cracks. *International Journal for Numerical Methods in Engineering, 57 (15),* 2221–2240. doi: https://doi.org/10.1002/nme.849
3. Moes, N., Dolbow, J., Belytschko, T. (1999). A finite element method for crack growth without remeshing. *International Journal for Numerical Methods in Engineering, 46 (1),* 131–150. doi: https://doi.org/10.1002/(sici)1097-0207(19990910)46:1<131::aid-nme726>3.0.co;2-j
4. Khoei, A. R. (2015). *Extended finite element method: theory and applications.* Chichester: John Wiley & Sons, Inc, 584.
5. Sukumar, N., Prévost, J.-H. (2003). Modeling quasi-static crack growth with the extended finite element method Part I: Computer implementation. *International Journal of Solids and Structures, 40 (26),* 7513–7537. doi: https://doi.org/10.1016/j.ijsolstr.2003.08.002
6. Nagashima, T., Wang, C. (2021). XFEM Analyses Using Two-Dimensional Quadrilateral Elements Enriched with Only the Heaviside Step Function. *International Journal of Computational Methods, 19 (2).* doi: https://doi.org/10.1142/s0219876221500638
7. Bansal, M., Singh, I. V., Mishra, B. K., Bordas, S. P. A. (2019). A parallel and efficient multi-split XFEM for 3-D analysis of heterogeneous materials. *Computer Methods in Applied Mechanics and Engineering, 347,* 365–401. doi: https://doi.org/10.1016/j.cma.2018.12.023
8. Agathos, K., Chatzi, E., Bordas, S. P. A. (2018). Multiple crack detection in 3D using a stable XFEM and global optimization. *Computational Mechanics, 62 (4),* 835–852. doi: https://doi.org/10.1007/s00466-017-1532-y
9. Ding, J., Yu, T., Bui, T. Q. (2020). Modeling strong/weak discontinuities by local mesh refinement variable-node XFEM with object-oriented implementation. *Theoretical and Applied Fracture Mechanics, 106,* 102434. doi: https://doi.org/10.1016/j.tafmec.2019.102434
10. Moës, N., Belytschko, T. (2002). Extended finite element method for cohesive crack growth. *Engineering Fracture Mechanics, 69 (7),* 813–833. doi: https://doi.org/10.1016/s0013-7944(01)00128-x
11. Dunant, C., Vinh, P. N., Belgasmia, M., Bordas, S., Guidoum, A. (2007). Architecture tradeoffs of integrating a mesh generator to partition of unity enriched object-oriented finite element software. *European Journal of Computational Mechanics, 16 (2),* 237–258. doi: https://doi.org/10.3166/remn.16.237-258
12. Rustum Mohsin, N., Shekher Jabur, L. (2019). Stress intensity factor for double edge cracked finite plate subjected to tensile stress. *University of Thi-Qar Journal for Engineering Sciences, 7 (1),* 101–115.
13. Sharma, K. (2014). Crack Interaction Studies Using XFEM Technique. *Journal of Solid Mechanics, 6 (4),* 410–421.
14. Jabur, L. S. (2015). Theorical and numerical analysis of central crack plate with different orientation under tensile load. *International Journal for Industrial Engineering and technology,* 2278–9456.
15. Dolbow, J., Moës, N., Belytschko, T. (2000). Modeling fracture in Mindlin–Reissner plates with the extended finite element method. *International Journal of Solids and Structures, 37 (48-50),* 7161–7183. doi: https://doi.org/10.1016/s0020-7683(00)00194-3
16. Hughes, T. J. R. (2000). *The finite element method: linear static and dynamic finite element analysis.* Mineola: Dover Publications, 704.
17. Clough, R. W., Penzien, J., Claudon, J.-L. (1980). *Dynamique des structures.* Paris: Éditions Pluralis, 752.
18. Belgasmia, M. (2021). *Structural dynamics and static nonlinear analysis from theory to application. Engineering Science Reference, an imprint of IGI Global.* Hershey, 347.
19. Smith, I. M., Griffiths, D. V., Margetts, L. (2014). *Programming the finite element method.* Chichester, John Wiley & Sons Inc, 684.
20. Bhatt, P. (2002). *Programming the Dynamic Analysis of Structures.* CRC Press, 464.

Sabah Moussaoui, *PhD, Department of Civil Engineering, Sétif 1 University, Sétif, Algeria, ORCID: https://orcid.org/0000-0002-8641-089X*

Chabane Rebadj, *Postgraduate Student, Department of Civil Engineering, Laarbi Tébessi University, Tébessa, Algeria, ORCID: https://orcid.org/0000-0002-6943-8807*

✉***Mourad Belgasmia,*** *Professor, Department of Civil Engineering, Sétif 1 University, Sétif, Algeria, e-mail: mourad.belgasmia@gmail.com, ORCID: https://orcid.org/0000-0003-1409-0281*

Kong Fah Tee, *Professor, Faculty of Engineering and Quantity Surveying, INTI International University, Nilai, Malaysia, ORCID: https://orcid.org/0000-0003-3202-873X*

✉*Corresponding author*